www.ijecs.in
International Journal Of Engineering And Computer Science ISSN: 2319-7242
Volume 7 Issue 10 October 2018, Page No. 24333-24341
Index Copernicus Value (2015): 58.10, 76.25 (2016) DOI: 10.18535/ijecs/v7i10.03

Detection of Cancer Nodules Using Transforms

Dr. Jinsa Kuruvilla[1], Sara Paul [2]

Department of Electronics and Communication
Mar Athanasius College of Engineering Kothamangalam, Kerala, India

Abstract:
In this paper, a computer aided detection of cancer nodules in Computed Tomography (CT) images of lungs using radon transform, ridgelet transform and Curvelet transform is proposed. The lung lobes are segmented from the CT images using morphological operations. The transforms are applied to the segmented lung lobes. From the transformed image, the presence of nodules in the lung lobes can be detected and located. The proposed detection method gives an accuracy of 98.5% with a sensitivity of 97.39% and specificity of 100%.

Introduction:

Many image processing tasks take advantage of sparse representations of image data where most information is packed into a small number of samples. Typically, these representations are achieved via invertible and non-redundant transforms. Currently, the most popular choices for this purpose are the wavelet transform and the discrete cosine transform. The success of wavelets is mainly due to the good performance for piecewise smooth functions in one dimension. Unfortunately, such is not the case in two dimensions. In essence, wavelets are good at catching zero-dimensional or point singularities, but two-dimensional piecewise smooth signals resembling images have one-dimensional singularities. That is, smooth regions are separated by edges, and while edges are discontinuous across, they are typically smooth curves (Thomas Arod, 2005). Intuitively, wavelets in two dimensions are obtained by a tensor-product of one dimensional wavelets and they are thus good at isolating the discontinuity across an edge, but will not see the smoothness along the edge. To overcome the weakness of wavelets in higher dimensions, three transforms are used in the chapter namely Radon transform, Ridgelet transform and Curvelet transform. The Radon transform detects the presence of nodule in the image, Ridgelet transform locates the position of the nodule and Curvelet transform segments the nodule from the image. By performing all these transforms, a cancer nodule location and shape can be automatically assessed without the help of a physician.

For detection of cancer, few methods have been reported in the literature. Bin Chen et al (2012) developed a segmentation method based on local intensity structure analysis and surface propagation in CT images. The average nodule detection rate is 95%. Niccolo Camarlinghi et al (2012) combined different computer aided detection methods to increase the actual support for radiologists in the identification of pulmonary nodules in CT scans. Binsheng Zhao et al (2003) proposed a three step approach for identification of nodules in multislice CT images. The three steps are separation of the lungs from the other anatomic structures, detection of nodule candidates in the extracted lungs and reduction of false-positives among the detected nodule candidates. The method achieved a

sensitivity of 84.2%. Matthew S. Brown et al (2001) proposed a patient specific model for automatic detection of pulmonary nodules with a sensitivity of 80%. Stefano Diciotti et al (2008) proposed a segmentation method based on 3D region growing by cropping the volume of interest enclosing the nodule. The sensitivity obtained is 86.5%. Jamshid Dehmeshki et. al (2008) proposed a 3D region growing with fuzzy connectivity to segment the nodules from CT images with a sensitivity of 84%. Xujiong Ye et al (2009) developed a shape based computer aided detection of lung nodules from CT images. The average detection rate obtained is 90.4%.

Radon Transform:

Radon transform is the process of projecting an image at different views (Tomasz Arod et al 2005). Radon transform is the projection of the intensity of an image along a radial line which is oriented at an angle. The value of a 2-D function at an arbitrary point is uniquely obtained by the integrals along the lines of all directions passing the point.

In mathematics, radon transform in two dimensions is the integral transform consisting of the integral of a function over straight lines. At each view, the gray scale matrix of each image becomes a vector. Each component in this vector corresponds to the line integral through the image. The number of projected vectors in each image is equal to the number of projected angles. The vector length is equal to 2*N-1 elements, where N is the maximum number of image pixels. The continuous Radon transform of an image $f(x,y)$ is given by

$$R(s,\theta) = \int_{-\infty}^{\infty}\int_{-\infty}^{\infty} f(x,y)\delta(x\cos\theta + y\sin\theta - s)dxdy \quad \text{- (6.1)}$$

$$-\infty < s < \infty, 0 \le \theta < \pi$$

Where $\delta(.)$ is the Dirac delta function and s = x.cos(θ) + y.sin(θ) defines the perpendicular distance of all lines in the image plane which form an angle θ∈[0,π] with respect to the x-axis. Radon transform of f (x,y) is the one dimensional projection of f (x,y) at an angle θ (Salim Lahmiri et al 2011).

In the rotated coordinate system (s,u), Radon transform can be expressed as

$$R(s,u) = \int_{-\infty}^{\infty} f(s\cos\theta - u\sin\theta, s\sin\theta + u\cos\theta)du$$

$$-\infty < s < \infty, 0 \le \theta < \pi$$

(6.2)

Where

$$s = x\cos\theta + y\sin\theta$$

(6.3)

$$u = -x\sin\theta + y\cos\theta$$

(6.4)

Radon transform represents the summation of f (x, y) along a ray at a distance s and at an angle θ. It maps the spatial domain (x, y) to the domain (s, u).

The Radon transform of an image is the sum of the Radon transforms of each individual pixel. The transform first divides pixels in the image into four subpixels and projects each subpixel separately. Each subpixel's contribution is proportionally split into the two nearest bins, according to the distance between the projected location and the bin centers. If the subpixel projection hits the center point of a bin, the bin on the axes gets the full value of the subpixel, or one-fourth the value of the pixel. If the subpixel projection hits the border between two bins, the subpixel value is split evenly between the bins.

Ridgelet Transform:

In ridgelet transform, the line singularity is mapped into point singularity using the Radon transform (Minh N. Do et al 2003). The wavelet transform is used to effectively handle the point singularity in the Radon domain. The ridgelet transform was introduced as a sparse expansion for functions on continuous spaces that are smooth

away from discontinuities along lines. Ridgelet transform has good directional selectivity and is able to locally and sparsely represent the signal when compared to the traditional transforms such as wavelet transform. As a new multiscale representation for functions on continuous spaces, it is smooth away from discontinuities along lines.

The ridgelet transform of an arbitrary bivariate function $f(x_1,x_2)$ in two dimensions is represented as

$$\psi_{a,b,\theta}(x) = a^{-\frac{1}{2}} f\left(\frac{x_1 \cos\theta + x_2 \sin\theta - b}{a}\right) \quad \text{--- (6.5)}$$

Where a > 0 is a scale parameter, θ is the orientation parameter and b is the location scalar parameter. The ridgelets are constants along lines $x_1 \cos\theta + x_2 \sin\theta$ and they are wavelets along the orthogonal direction. Using common θ and b and different scales for a, it is possible to efficiently approximate the singularities along a line. The ridgelet coefficients of an integrable bivariate function f(x) is defined as

$$R_f(a,b,\theta) = \int \psi_{a,b,\theta}(x) f(x) dx \quad \text{--- (6.6)}$$

The reconstruction is given by

$$f(x) = \int_0^{2\pi} \int_{-\infty}^{\infty} \int_0^{\infty} R_f(a,b,\theta) \psi_{a,b,\theta}(x) \frac{da}{a^3} db \frac{d\theta}{4\pi} \quad \text{--- (6.7)}$$

Wavelets are very effective in representing objects with isolated point singularities, while ridgelets are very effective in representing objects with singularities along lines (E. J. Candes, 1998). In fact, ridgelets is a way of concatenating 1-D wavelets along lines. In 2-D, points and lines are related via the Radon transform, thus the wavelet and ridgelet transforms are linked using the Radon transform. The ridgelet transform is the application of a 1-D wavelet transform to the slices (also referred to as projections) of the Radon transform (E. J. Candes et al 1999).

The continuous ridgelet transform is expressed as

$$CRT_f(a,b,\theta) = \int_R \psi_{a,b}(t) R_f(\theta,t) dt \quad \text{---- (6.8)}$$

The relation between radon transform and ridgelet transform is shown in Figure 6.1

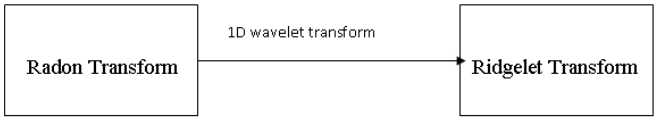

Figure 6.1: Relation between radon transform and ridgelet transform:

The basic strategy for calculating the continuous ridgelet transform is first to compute the Radon transform and second, to apply a one-dimensional wavelet transform to the slices.

Curvelet Transform:

Curvelet transform is a non-adaptive technique for multi scale object representation and an appropriate basis for representing images which are smooth apart from singularities along smooth curves, where the curves have bounded curvature (Shadi Al Zubi et al 2011). Curvelet transform is a new multi-scale representation most suitable for objects with curves. The continuous curvelet transform can be defined by a pair of windows W(r) (a radial window) and V(t) (an angular window), with variables Was a frequency-domain variable, and r and t as polar coordinates in the frequency-domain.

$$\sum_{j=-\infty}^{\infty} W^2(2^j r) = 1 \quad \text{--- (6.9)} \qquad r \in \left(\frac{3}{4}, \frac{3}{2}\right)$$

$$\sum_{j=-\infty}^{\infty} V^2(t-1) = 1 \quad \text{--- (6.10)} \qquad t \in \left(-\frac{1}{2}, \frac{1}{2}\right)$$

The curvelet transform can be defined as a function of x =(x1, x2) at scale 2^{-j}, orientation θ_l, and position $x_k^{(j,l)}$ by

$$\varphi_{j,l,k}(x) = \varphi_j(R_{\theta_l}(x - x_k^{(j,l)})) \quad \text{---- (6.11)}$$

Where R_θ is the rotation in radians. Implementation of curvelet transform involves the following steps:

1) Subband Decomposition
2) Smooth Partitioning
3) Renormalization
4) Ridgelet Analysis

Subband decomposition: The object f is filtered into subbands.

$$f = (P_0 f, \Delta_1 f, \Delta_2 f .....) \quad \text{--- (6.12)}$$

P_0 is low pass filter and Δ_1, Δ_2 are band pass filters. The original image can be reconstructed from the subbands by

$$f = P_0(P_0 f) + \sum_s \Delta_s(\Delta_s f) \quad \text{---- (6.13)}$$

Smooth Partitioning: Each subband is smoothly windowed into "squares" of an appropriate scale (Jean-Luc Starck et al 2002).

$$\Delta_1 f = W_Q \Delta_s f, Q \in Q_s \quad \text{---- (6.14)}$$

Where Q is a dyadic square. The notation Q_s will correspond to all dyadic squares of scale s. Let W_Q be a window centered near Q, obtained after dilation and translation of a single w, such that the $W_Q^2, Q \in Q_s$ make up a partition of unity.

Renormalization: Each resulting square is renormalized to unit scale. The multiscale ridgelet system renormalizes and transports the ridgelet basis method and makes it as a system of elements at all lengths and all finer widths (Jianwei Ma et al 2010).

$$g_Q = (T_Q)^{-1}(W_Q \Delta_s f), Q \in Q_s \quad \text{--- (6.15)}$$

Ridgelet Analysis: The orthonormal ridgelet transform is applied to each square.

Experimental Results:

The Radon transform indicates the presence of nodule in the image. An approximate location of the nodule can be obtained from the radon transform. The correct location is given by the Ridgelet transform output. The Ridgelet output is able to give an approximate shape of the nodule. The exact shape of the nodule is given by Curvelet transform. From the curvelet transformed image, the nodule can be segmented correctly. The nodules are classified as malignant or benign based on shape parameters and texture parameters.

Figure 6.2 and Figure 6.3 show a CT image of lungs without cancer nodule and its segmented output respectively.

Figure 6.2: CT image of lungs without cancer nodule

Figure 6.3: Segmented output of Figure 6.2

The radon transformation is applied to the segmented lung lobe. The radon transform output of Figure 6.3 is shown in Figure 6.4. In the transform, there is no intensity distribution indicating that there is no specific change or abnormality as compared to normal lungs.

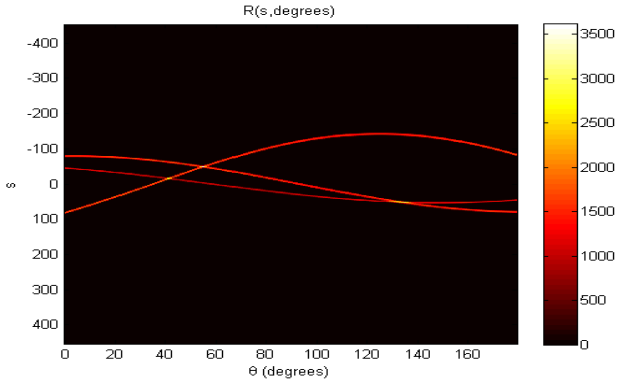

Figure 6.4: Radon transform of Figure 6.3

Detection of Nodule:

Figure 6.5 and Figure 6.6 show a CT image of lungs with well circumscribed nodule located in right lung lobe and its segmented output respectively.

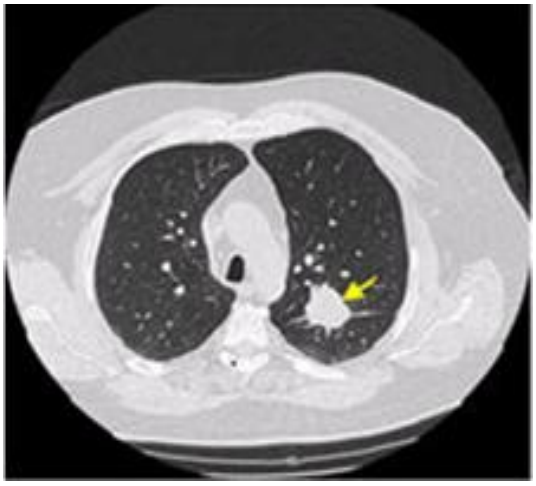

Figure 6.5: CT image with well circumscribed nodule in right lung lobe

Figure 6.6: Segmented output of Figure 6.5

The radon transform output of Figure 6.6 is shown in Figure 6.7. The presence of nodule in left lung or in right lung can be detected from transformed output.

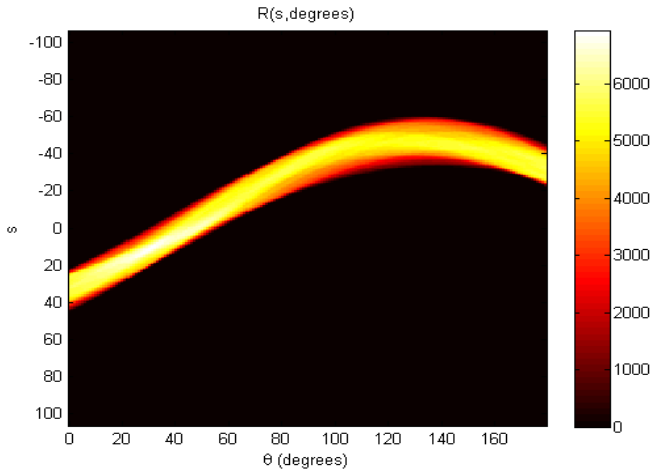

Figure 6.7: Radon transform of Figure 6.6

The 2D transform shows that the curve is bending towards the right side. The curve bending shows that towards right side of the image, the intensity distribution is more. This indicates that the cancer nodule is located in the right lung lobe. The radon transform output indicates the presence of nodules in the CT images. To locate the position of nodules, radon transform plots are taken at angle 0^o and angle 90^o. At angle 0^o and angle 90^o the distance in the transformed output is equivalent to the pixel distance. The radon transform at $\theta = 0^\circ$ is represented as X detail and the radon transform at $\theta = 90^\circ$ is represented as Y detail. When $\theta = 0^\circ$, the equation 6.2 and 6.3 reduce to

$$s = x$$
$$u = y \qquad \text{--- (6.16)}$$

$$\begin{bmatrix} s \\ u \end{bmatrix} = \begin{bmatrix} x \\ y \end{bmatrix} \qquad \text{--- (6.17)}$$

The equation 6.16 shows that the distance in X detail is equal to the pixel distance in image. The x-axis of the X detail plot shows the distance at which the nodule is located.

When $\theta = 90^\circ$, equation 6.2 and 6.3 reduce to

$$s = y$$
$$u = -x \quad \text{--- (6.18)}$$

$$\begin{bmatrix} s \\ u \end{bmatrix} = \begin{bmatrix} y \\ -x \end{bmatrix} \quad \text{--- (6.19)}$$

The distance in Y detail is also equal to the pixel distance of the image. The x-axis of the Y detail plot shows the distance at which the nodule is located. From Figure 6.7, it is indicated that the nodule is present in the right lung of Figure 6.6. To locate the position of the nodule in Figure 6.6, the right lung is segmented and radon transform is performed. Figure 6.8 and Figure 6.9 show the Y detail and X detail plots of Figure 6.6 respectively.

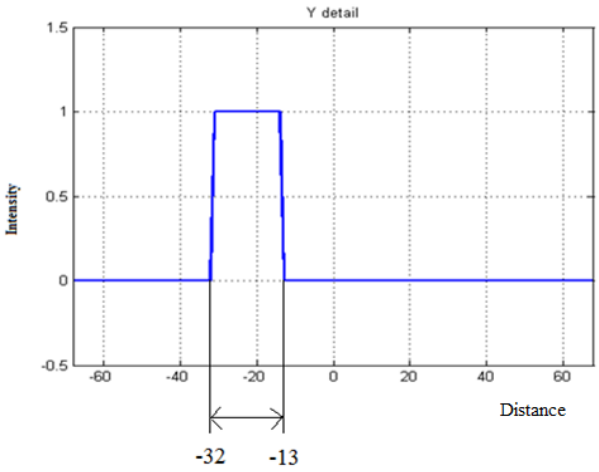

Figure 6.8: Y detail plot of Figure 6.6

In the Y detail plot, the distribution of the intensity is in the negative side. It indicates that the nodule is located below the center part of the lungs in y-axis. The nodule spread is from pixel distance 13 to 32 below the origin in y-axis. In X detail plot, the distribution of intensity is on both side of origin. This indicates that the nodule is located in the center part of the lungs in x-axis. The nodule spread is from 0 to 15 pixel distances to the left side and 0 to 5 pixel distances to the right side. Analyzing X detail and Y detail plots, it can be concluded that the nodule is located in the lower part of the right lungs and in the lower part; the nodule is located at the center.

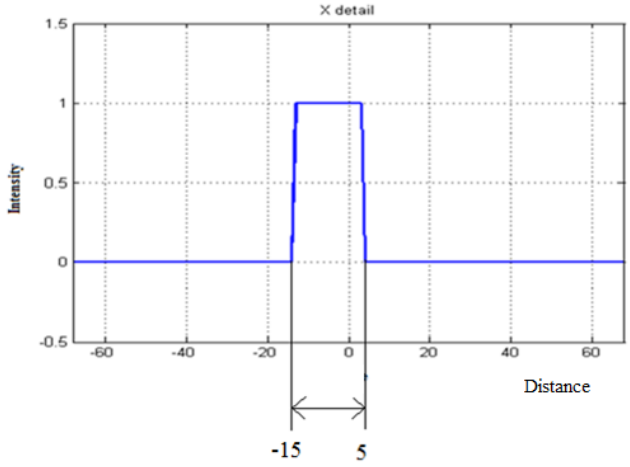

Figure 6.9: X detail plot of Figure 6.6

The correct location of the nodule is given by the ridgelet transform output. The ridgelet output is able to give the shape of the nodule. The ridgelet transform output of Figure 6.6 is shown in Figure 6.10 and Figure 6.11. The X level shows the ridgelet output when $\theta = 0^{\circ}$ for the radon transform output. The Y level shows the ridgelet output when $\theta = 90^{\circ}$ for the radon transform output.

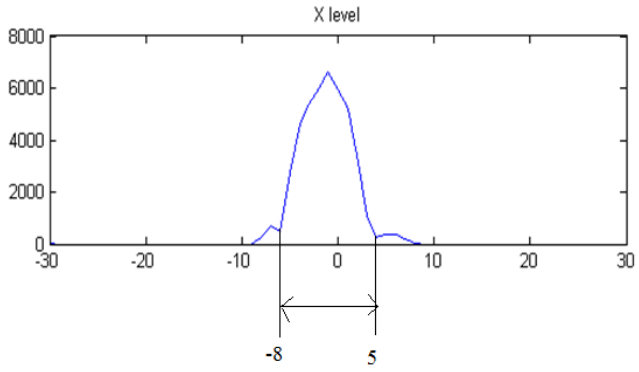

Figure 6.10: Ridgelet output at θ = 0°

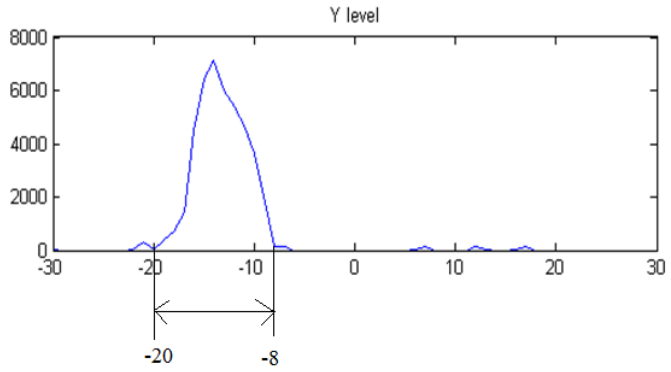

Figure 6.11: Ridgelet output at θ = 90^o

From Figure 6.10 and Figure 6.11 the location of the nodule is found as:

In the Y axis below the origin from 8 to 20 pixel distance

In the X axis on either side of origin: left side 8 pixel distance and right side 5 pixel distance

To find the exact shape of the nodule, the curvelet transform is performed. The curvelet transformed output of Figure 6.6 is shown in Figure 6.12.

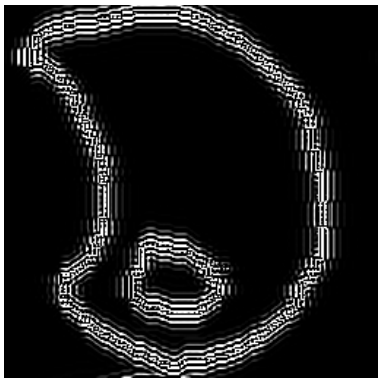

Figure 6.12: Curvelet output

The nodule can be segmented from the Curvelet output by separating the connected components in the curves. The curve with more number of connected components is the lungs itself and it is removed to get the nodule as final output. The final segmented nodule is shown in Figure 6.13.

Figure 6.13: Segmented nodule

Radon transform indicates that nodule is present in the right lung, Ridgelet transform finds the exact location of the nodule and Curvelet transform segments the nodule from the image.

Conclusion:

In this paper, a computer aided detection and classification of nodule in CT images of lungs is proposed. In the first phase of the proposed technique, the lung region is extracted from the image using morphological operations. Then 2D radon transform is applied to detect whether the nodule is present in left lung or in right lung. An approximate location of the nodule is detected by the radon transform at angle 0^o and angle 90^o. The correct location of the nodule is given by the ridgelet transform output. The ridgelet output is able to give an approximate shape of the nodule. The nodule can be segmented from the curvelet transform output. The proposed detection method gives an accuracy of 98.5% with a sensitivity of 97.39% and specificity of 100%. The images in which small nodules located at the pleural side near the sternum are not detected correctly. In these cases the proposed detection method is not able to differentiate between the nodule and the sternum present in the image.

References:

[1] Bin Chen and Takayuki Kitasaka 2012, 'Automatic segmentation of pulmonary blood vessels and nodules based on local intensity structure analysis and surface propagation in 3D chest CT images' International Journal of Computer Assisted Radiology and Surgery, vol 7, pp. 465–482.

[2] Zhao B, Gamsu G, Ginsberg MS, Jiang L and Schwartz LH 2003, ' Automatic detection of small lung nodules on CT utilizing a local density maximum algorithm' Journal of Applied Clinical Medical Physics, vol. 4, no. 3, pp. 248-260.

[3] Matthew S. Brown, Mc Nitt Gray M F, Goldin J G, Suh RD, Sayre JW and Aberle 2001, 'Patient-Specific Models for Lung Nodule Detection and Surveillance in CT Images', IEEE Transactions on Medical Imaging, vol. 20, no. 12, pp. 1242-1250.

[4] Stefano Diciotti, Picozzi G, Falchini M, Mascalchi M, Villari N and Valli G 2008, '3-D Segmentation Algorithm of Small Lung Nodules in Spiral CT Images', IEEE Transactions on Information Technology In Biomedicine, vol. 12, no. 1, pp. 7-19.

[5] Jamshid Dehmeshki, Amin H, Valdivieso M and Ye X 2008, 'Segmentation of Pulmonary Nodules in Thoracic CT Scans: A Region Growing Approach' IEEE Transactions on Medical Imaging, vol. 27, no. 4, pp. 467-480.

[6] Xujiong Ye and Xinyu Lin july 2009, 'Shape-Based Computer-Aided Detection of Lung Nodules in Thoracic CT Images', IEEE Transactions on Biomedical Engineering, vol. 56, no. 7, pp. 1810-1820.

[7] Tomasz Arod 2005, 'Invariant Object Recognition Using Radon-Based Transform', Computing and Informatics, vol. 24, pp. 183–199.

[8] Salim Lahmiri and Mounir Boukadoum 2011, 'Hybrid Cosine and Radon Transform-based processing for Digital Mammogram Feature Extraction and Classification with SVM', 33rd Annual International Conference of the IEEE EMBS, Boston, Massachusetts USA, pp.

[9] E. J. Candes 1998, Ridgelets: Theory and applications, Ph.D. dissertation, Dept. Statistics, Stanford University, Stanford, CA.

[10] E. J. Candès and D. L. Donoho 1999, 'Ridgelets: A key to higher-dimensional intermittency,' Philosophical Transactions of Royal Societyof London, pp. 2495–2509.

[11] Minh N. Do and Martin Vetterli 2003, 'The Finite Ridgelet Transform for Image Representation', IEEE Transactions on Image Processing, vol. 12, no. 1, pp. 16-28.

[12] Shadi AlZubi, Naveed Islam, and Maysam Abbod 2011, 'Multiresolution Analysis UsingWavelet, Ridgelet, and Curvelet Transforms for Medical Image Segmentation', International Journal of Biomedical Imaging, Hindawi Publishing Corporation, pp. 1-19.

[13] Jean-Luc Starck, Emmanuel J. Candès, and David L. Donoho June 2002, 'The Curvelet Transform for Image Denoising', IEEE Transactions On Image Processing, vol. 11, no. 6, pp. 670 - 684.

[14] Jianwei Ma and Gerlind Plonka March 2010, 'The Curvelet Transform', IEEE Signal Processing Magazine, pp. 118-133.

[15] Shingo Iwano, Tatsuya Nakamurab, Yuko Kamiokac, Mitsuru Ikeda and Takeo Ishigaki 2008, 'Computer-aided differentiation of malignant from benign solitary pulmonary nodules imaged by high-resolution CT', Computerized Medical Imaging and Graphics, vol. 32, pp. 416–422.

[16] Yang X.U, Liu Jia, Hu Qingmao, Chen Zhijun, Du Xiaohua and Heng Pheng Ann 2008, 'F-score Feature Selection Method May Improve Texture-based Liver Segmentation Strategies', Proceedings of IEEE International Symposium on IT in Medicine and Education, pp. 697-702.

[17] Verma B, P. McLeod and A. Klevansky 2010, 'Classification of benign and malignant patterns in digital mammograms for the diagnosis of breast cancer', Expert Systems with Applications, vol. 37, pp. 3344–3351.

[18] Qiao Wei, Yaoping Hu, Gary Gelfand, and John H. MacGregor May 2009, 'Segmentation of Lung Lobes in High-Resolution Isotropic CT Images', IEEE Transactions on Biomedical Engineering, vol. 56, no. 5, pp. 1383- 1393.

[19] Russell C. Hardie, Steven K. Rogers, Terry Wilson and Adam Rogers 2008, 'Performance analysis of a new computer aided detection system for identifying lung nodules on chest radiographs', Medical Image Analysis, vol. 12, pp. 240–258.

Cascio D, Magro R, Fauci F, Iacomi M and Raso G 2012, 'Automatic detection of lung nodules in CT datasets based on stable 3D mass–spring models', Computers in Biology and Medicine, vol. 42, pp. 1098–1109.